

# How ions in solution can change the sign of the critical Casimir potential

Faezeh Pousaneh,<sup>1</sup> Alina Ciach,<sup>1</sup> and Anna Maciołek<sup>2,3,1</sup>

<sup>1</sup>*Institute of Physical Chemistry, Polish Academy of Sciences,*

*Kasprzaka 44/52, PL-01-224 Warsaw, Poland*

<sup>2</sup>*Max-Planck-Institut für Intelligente Systeme,*

*Heisenbergstraße 3, 70569 Stuttgart, Germany*

<sup>3</sup>*IV. Institut für Theoretische Physik, Pfaffenwaldring 57,*

*Universität Stuttgart, D-70569 Stuttgart, Germany*

## Abstract

We show that hydrophilic ions present in a confined, near-critical aqueous mixture can lead to an attraction between like charge surfaces with opposing preferential adsorption of the two species of the mixture, even though the corresponding Casimir potential in uncharged systems is repulsive. This prediction agrees with recent experiment [Nellen *et al.*, Soft Matter **80**, 061143 (2011)]. We also show that oppositely charged hydrophobic surfaces can repel each other, although the Casimir potential between uncharged surfaces with like preferential adsorption (selectivity) is attractive. This behavior is expected when the electrostatic screening length is larger than the correlation length, and one of the confining surfaces is strongly selective and weakly charged, whereas the other confining surface is weakly selective and strongly charged. The Casimir potential can change sign because the hydrophilic ions near the weakly hydrophobic surface can overcompensate the effect of hydrophobicity, and this surface can act as a hydrophilic one. We also predict a more attractive interaction between hydrophilic surfaces and a more repulsive interaction between hydrophobic surfaces than given by the sum of the Casimir and Debye-Hückel potentials. Our theory is derived systematically from a microscopic approach, and combines the Landau-type and Debye-Hückel theories with an additional contribution of an entropic origin.

## I. INTRODUCTION

Properties of colloidal systems depend crucially on effective interactions between the colloid particles [1, 2]. For this reason a possibility of tuning these interactions by reversible changes of some control parameter is of a great interest in a colloidal science. Temperature is a thermodynamic parameter that can be easily changed in a reversible manner, therefore temperature controlled thermodynamic Casimir potential draws an increasing attention [3–7]. An importance of the Casimir potential follows also from the fact that its range is given by the bulk correlation length, which diverges at the critical point of the fluid confined between the particles. Recent experimental studies [8] suggest that also Nature seems to take advantage of the Casimir potential in life processes. The multicomponent lipid membranes in living organisms are close to the critical demixing point [9, 10], which should lead to the Casimir potential between membrane proteins or other large inclusions. A very long range of attraction may explain why despite a very low concentration of the macromolecules, their aggregates can be formed.

### A. The Casimir potential

The thermodynamic Casimir forces arise near the critical point of a fluid confined between two surfaces (e.g. surfaces of particles) as a result of critical fluctuations and they act between the confining surfaces [3, 4, 11–14]. The critical point can be associated with: (i) a gas-liquid phase separation, (ii) in the case of complex fluids, e.g. colloidal suspensions with solvents including polymers or micelles, with a separation into phases poor and rich in these, so called depletion agents [15], (iii) or with a demixing transition in a binary or multicomponent mixture [3–5, 7, 16]. In the latter two cases, the critical temperature may be close to the room temperature. The emergence of the Casimir interactions is directly related to the phenomenon of critical adsorption [11, 12] at the confining surfaces. For an adsorbing surface, there is an excess density of the fluid in a surface layer of a thickness comparable with the bulk correlation length  $\xi$ . When the critical point with the critical temperature  $T_c$  is approached, then the bulk correlation length increases,  $\xi = \xi_0 |\tau|^{-\nu}$ , where  $\tau = (T - T_c)/T_c$ ,  $\nu \approx 0.63$  for the three dimensional ( $d = 3$ ) Ising universality class, and  $\xi_0$  is a material constant of the order of few Angstroms [4, 6, 17]. In the case of the demixing transition, a

layer rich in the component  $A$  ( $B$ ) is formed near the surface preferentially adsorbing the  $A$ -type molecules ( $B$ -type molecules). When the distance between the two surfaces is  $L \sim \xi$ , then the adsorbed layers overlap and influence each other. The  $L$ -dependent modification of the density or concentration profile leads in turn to the  $L$ -dependent excess grand potential, i.e. the excess pressure. Surfaces with the like adsorption preferences attract each other, whereas opposing adsorption preferences lead to a repulsion [3, 4, 13, 14, 18]. Close to the critical point, the potential of the Casimir force is universal. It has a scaling form with a scaling function which is the same for surfaces with similar adsorption preferences, and the same for surfaces with opposite adsorption preferences, independently of the strength of the surface-fluid interaction  $h_1$ . For  $L/\xi > 1$  the Casimir potential per unit area between parallel surfaces decays exponentially,  $\beta V_C(L) = \pm \frac{A_c}{\xi} \exp(-L/\xi)$ , with different values of the amplitude  $A_C$  for like and unlike surfaces. One should note, however that the temperature range  $|\tau|$  corresponding to the universal behavior shrinks with decreasing  $h_1$  [19, 20]. In the case of weakly adsorbing surfaces, the Casimir potential can depend on  $h_1$  for experimentally accessible range of  $\tau$  [18–21].

## B. The sum of the Casimir and electrostatic interactions

In systems such as the colloidal suspensions, the van der Waals and electrostatic interactions between the colloidal particles are also present. The former can be eliminated by a refractive-index matching. The latter can be screened by adding salt to the solution. In the case of two parallel charged surfaces with surface charges  $e\sigma_0$  and  $e\sigma_L$  in the solution containing ions, the electrostatic potential per unit area between them decays exponentially for large separations,  $\beta V_{el}(L) \simeq \frac{2\kappa\sigma_0\sigma_L}{\bar{\rho}_{ion}} \exp(-\kappa L)$ .  $e$  is the elementary charge,  $\kappa$  is the inverse Debye screening length and  $\bar{\rho}_{ion}$  is the number density of ions [17, 22]. When the screening length  $1/\kappa$  is comparable with  $\xi$ , then the electrostatic repulsion between like surfaces competes with the Casimir attraction. The sum of the two potentials,

$$\beta V(L) = -\frac{A_C}{\xi} \exp(-L/\xi) + \frac{2\kappa\sigma_0\sigma_L}{\bar{\rho}_{ion}} \exp(-\kappa L), \quad (1)$$

depends on the ratio of the decay rates

$$y = \xi\kappa \quad (2)$$

and on the ratio of the amplitudes,  $\frac{y\sigma_0\sigma_L}{\rho_{ion}A_C}$ . In the critical region and for small salt content, the two lengths are large,  $\xi, 1/\kappa \gg a$ , where  $a$  is the molecular size. The interesting phenomena occur if the separation between the surfaces is comparable with the two relevant length scales,  $L \sim \xi, 1/\kappa$ . The potential per unit area between curved surfaces of colloid particles differs from (1), but has the same qualitative features. For distances between the surfaces much smaller than the particles radii the form of the potential can be obtained in the Derjaguin approximation [4, 23].

Let us discuss the effective interactions arising from the sum in Eq. (1) for the case of identical surfaces. When the correlation length is larger than the screening length ( $y > 1$ ) and the surface charge is large, a repulsion at small separations  $L$  crosses over to an attraction at large  $L$ , so that  $V(L)$  has a minimum for  $L \sim \xi$ . For surfaces with an area typical for colloid particles, the depth of the minimum can be as large as a few  $k_B T$ , which is enough for inducing phase transitions [7]. On the other hand, for  $y < 1$  and for small  $\frac{y\sigma_0\sigma_L}{\rho_{ion}A_C}$ , it follows from Eq. (1) that the Casimir attraction at small separations  $L$  crosses over to the electrostatic repulsion at large  $L$ . If the emerging repulsion barrier between the colloid particles is sufficiently strong, the phase separation in the particle-rich and particle-poor phases due to the Casimir attraction between particle surfaces [7] is suppressed. The resulting short-range attraction long-range repulsion (SALR) effective potential can lead to the formation of dynamic spherical or elongated clusters, a network or layers of particles [24–29].

On the other hand, in the case of oppositely charged surfaces with opposing preferential adsorption, e.g., hydrophilic and hydrophobic surfaces, the Casimir potential is repulsive whereas the Coulomb potential is attractive (in this case  $A_C < 0$  and  $\sigma_0\sigma_L < 0$  in (1)). The sum of the two potentials can have a minimum or a maximum for separations  $L \sim \xi$ , depending on  $y$  and on  $\frac{y\sigma_0\sigma_L}{\rho_{ion}A_C}$ . By varying the temperature and thereby changing the bulk correlation length  $\xi$ , one can cause the attractive well or the repulsive barrier in the effective potential to appear and to disappear. Thus it seems possible to induce or to suppress a macro- or microphase separation by small temperature changes. Indeed, analogs of the gas, liquid and crystal phases were induced and destroyed by temperature changes within  $0.5C$  [7].

It seems that it is not enough to just add the Casimir and the screened electrostatic potential in order to obtain the effective interactions between the surfaces. The total potential can

strongly deviate from the sum of the Casimir and the electrostatic potentials, even when no other interactions are present. The experimental results obtained in Ref.[4] for  $y > 1$  could not be fitted with Eq. (1). Only for distances much larger than the position of the potential minimum it was possible to fit the universal Casimir potential with the experimental results, because for  $y > 1$  and  $\kappa L \gg 1$  the electrostatic contribution is negligible. In another experiment [6] an attraction was measured between like charge hydrophilic and hydrophobic surfaces for some temperature range corresponding to  $y < 1$ . Both the electrostatic and the Casimir potentials are repulsive, and according to Eq. (1) should lead together to enhanced repulsion. The experimental result of Ref.[6] is in complete disagreement with Eq. (1). The above strong quantitative [4] and even qualitative [6] disagreement between Eq. (1) and the experiment show that in order to design effective interactions it is necessary to develop a more accurate theory. Several attempts have been made already, see Ref. [30–36].

### C. An interplay of Casimir and electrostatic interactions

The critical point in Ref.[3, 4, 6] was associated with the water-lutidine phase separation. In Ref.[3, 4] the ions come from dissociation of water, and in Ref.[6],  $KBr$  was added. A solubility of the ions in water is much bigger than in the lutidine. The water-rich phase is thus rich in ions, whereas the lutidine-rich phase is poor in ions. As mentioned in the passing, near the hydrophobic surface an excess of lutidine in a layer of thickness  $\sim \xi$  is predicted by the theory of critical adsorption [11–14]. If this surface is charged, then the excess number density of ions in a layer of thickness  $1/2\kappa$  is predicted by the Debye-Hückel theory [37]. However, because of much lower solubility of the ions in lutidine than in water, a simultaneous excess density of lutidine and of ions near the surface is associated with a large internal-energy penalty. The distribution of the ions as well as the solvent composition near the surface must be a compromise between the bulk tendency to separate the ions from the lutidine, and the surface preference to attract both immiscible components. As found in Ref.[31], when  $y < 1$  a thin lutidine-rich layer can be formed at the hydrophobic surface, but this layer is followed by a layer rich in water and ions. Thus, in the critical region the charged hydrophobic surface behaves as an *effectively hydrophilic* one. The Casimir potential between hydrophilic surfaces is attractive. For this reason weakly charged surfaces can attract each other.

The above physical picture is consistent with the theory developed in Refs.[30–32]. The theory was derived from a microscopic lattice gas model for a four component mixture, and also from a simple density functional theory (DFT). We took into account van der Waals (vdW) type of interactions between all the components in addition to the Coulomb interactions between the ions. We have assumed that the vdW interactions between the cation and a given specie is the same as the vdW interaction between the anion and this specie. Similar assumption was made for the interactions with the surfaces.

After a systematic coarse-graining procedure appropriate in the critical region, a Landau-type functional, containing also the electrostatic energy contribution was obtained. In this theory the dominant contribution to the effective interaction between the surfaces is similar to Eq. (1). However, because of the mutual influence of the solvent composition and the charge distribution,  $\sigma_0\sigma_L$  and  $A$  should be replaced by the amplitudes that both depend on surface charges, fluid-wall interactions and on the ratio of the decay lengths  $y$ . Moreover, additional terms,  $\propto \exp(-2\kappa L)$  for  $y < 1$  and  $\propto \exp[-L(\kappa + 1/\xi)]$  for  $y > 1$  should be included. For  $y > 1$ , corresponding to the experiment in Ref.[3], a satisfactory quantitative agreement was obtained for 4 different combination of surfaces in Ref.[32]. Unfortunately, the fluid-wall interactions could not be determined experimentally, and were used as fitting parameters. Importantly, in each case the best fits were obtained for  $\xi_0 = 0.2nm$ , in perfect agreement with recent measurements [6] by the same group that performed the experiment in Ref.[3].

There were other attempts to explain the discrepancies between Eq. (1) and the experimental results [33, 36]. In Refs. [33, 36] the phenomenological Landau-type functional was developed by adding the Landau functional for the critical solvent and the free energy of the ions. In addition, terms describing the coupling of the density of the anions and the cations with the solvent composition were included. The unusual attraction between like charge hydrophilic and hydrophobic surfaces was obtained in these theories as a result of different solubility of the anion and the cation in water, and different interactions of the two ionic species with the surfaces.

Presumably both effects play some role in experiments [6]. Since only our theory agrees quantitatively with the experiment [4], we believe that it captures the key physical phenomena of the confined near-critical mixture containing ions with preferential solubility in one of the solvent components.

The preliminary results presented in Ref.[31] concerned only like charge hydrophilic and hydrophobic surfaces, as in the experimental studies [6]. In this work a systematic and complete analysis of all possible combination of selectivity and surface charges of the two confining surfaces is presented within the theory developed in Refs.[30–32]. The theory is further simplified, and in the new version the essential physics is amplified. We introduce the order parameter (OP) suitable for the phase separation into a phase rich in water and ions, and a phase rich in lutidine and poor in ions.

Our presentation is organized as follows. We introduce the new version of the theory in Sec. II. In Sec. III we derive and analyze approximate analytical expressions for  $y < 1$ . In particular, we show that oppositely charged surfaces with similar adsorption preferences can repel each other for some range of  $y$  even though both terms in (1) are attractive. Comparison with numerical results is shown in Sec. V for a few representative cases. Sec. VI contains summary and discussion.

## II. THE GENERIC MODEL

We consider a four-component mixture between parallel walls. In equilibrium, when temperature and chemical potentials are fixed, the distribution of the components in the slit corresponds to the minimum of the grand potential

$$\Omega = A\omega = A\left[u_{vdW} + u_{el} - Ts - \int_0^L dz \mu_i \rho_i(z)\right]. \quad (3)$$

$A$  is the area of the surfaces separated by the distance  $L$ ,  $S = As$  denotes entropy,  $\rho_i(z)$  and  $\mu_i$  are the local number density and the chemical potential of the  $i$ -th component, respectively, with  $i = w, l(1, 2)$  corresponding to water and organic solvent (lutidine here), and  $i = +, -(3, 4)$  corresponding to the cation and the anion. Summation convention for repeated indexes is assumed. Due to the charge neutrality  $\mu_+ = \mu_-$ . We consider dimensionless distance and dimensionless  $\rho_i$ , i.e. length is measured in units of  $a$ , and  $\rho_i = a^3 N_i/V$ , where  $a^3$  is the average volume per particle in the liquid phase, and  $N_i$  denotes the number of the  $i$ -th kind particles in the volume  $V$ . We neglect compressibility of the liquid and assume that the total density is fixed,

$$\sum_{i=1}^4 \rho_i = 1. \quad (4)$$

The microscopic details, in particular different sizes of molecules are disregarded, since we are interested in the density profiles on the length scale much larger than  $a$ .

The electrostatic energy per surface area is given by [17, 30, 32]

$$u_{el} = \int_0^L dz \left[ -\frac{\epsilon}{8\pi} (\nabla\psi)^2 + e\rho_q\psi \right] + e\sigma_0\psi(0) + e\sigma_L\psi(L), \quad (5)$$

where  $\psi$  is the electrostatic potential which satisfies the Poisson equation

$$\nabla^2 \psi(z) = -\frac{4\pi e}{\epsilon} \rho_q(z), \quad (6)$$

with the Neumann boundary conditions (BC),

$$\nabla \psi(z)|_{z=0} = -\frac{4\pi e}{\epsilon} \sigma_0, \quad \nabla \psi(z)|_{z=L} = \frac{4\pi e}{\epsilon} \sigma_L, \quad (7)$$

appropriate in the case of fixed surface charges. In the above  $\epsilon$  is the dielectric constant,  $e\sigma_0$  and  $e\sigma_L$  are the surface charges at the two walls, and

$$e\rho_q(z) = e(\rho_+(z) - \rho_-(z)) \quad (8)$$

is the charge density.

Finally,  $U_{vdW} = Au_{vdW}$  is the contribution to the internal energy associated with the vdW interactions between all the components. Because of the universality of critical phenomena, the detailed form of the interactions is irrelevant. The density profiles at the length scale  $\xi \gg a$  can be obtained from highly simplified models, such as the lattice gas model of a mixture, where only nearest-neighbors interact with the coupling constant  $J_{ij}$  between the  $i$ -th and  $j$ -th components. In continuous models the relevant energy parameter is  $J_{ij} = \frac{1}{2d} \int d\mathbf{r} V_{ij}(r)$ , where  $V_{ij}(r)$  is the interaction potential between the  $i$ -th and  $j$ -th component, and  $d$  is the space dimension. Solubility of inorganic ions in water is much higher than in organic solvent. We can expect that the vdW interaction between the cation and a given specie is similar to the vdW interaction between the anion and this specie. In Refs. [30–32] it was assumed that  $J_{+i} = J_{-i}$ . Here we make further simplifying assumptions. The mixture separates into a phase rich in water and ions, and a phase rich in lutidine and poor in ions. From the point of view of the phase separation water and ions play the similar role, and the vdW interactions between water and a given specie should be comparable to the vdW interactions between the ion and this specie. We thus make additional assumption,



$J_{wi} = J_{+i} = J_{-i}$ . In the critical region we can perform the coarse-graining procedure as described in Ref.[30], and after some algebra obtain the vdW contribution to the internal energy (up to a constant) of the form

$$u_{vdW}/J = \int_0^L \left[ -d\Phi^2 + \frac{1}{2}(\nabla\Phi)^2 \right] dz + \frac{1}{2} \left( \Phi(0)^2 + \Phi(L)^2 \right) - h_0\Phi(0) - h_L\Phi(L), \quad (9)$$

where

$$\Phi(z) = \rho_w(z) + \rho_{ion}(z) - \rho_l(z) \quad (10)$$

is the critical order parameter(OP), and

$$\rho_{ion}(z) = \rho_+(z) + \rho_-(z), \quad (11)$$

is the number density of ions,  $h_0$  and  $h_L$  are the interactions with the surfaces in  $J$ -units, and  $J = \frac{1}{4}(J_{ww} + J_{ll} - 2J_{wl})$  is the single energy parameter relevant for the phase separation. Note that since in the phase separation water and ions play similar roles (both prefer the same phase),  $\Phi$  is the natural OP for this phase transition. In the absence of ions  $\Phi$  reduces to the order parameter of the symmetrical binary mixture,  $\rho_w - \rho_l$ , and vanishes at the critical demixing point. Real mixtures are not symmetrical, and the OP (10) should be replaced by  $\Phi(z) - \bar{\Phi}$ , where  $\bar{\Phi}$  is the bulk critical value. However, the effective potential between confining surfaces depends on the deviations of the composition from its critical value and not on this value itself. For this reason the symmetrical mixture or the lattice gas model are commonly used in studies of critical phenomena. We make the same assumption here, and in our symmetrical mixture  $\Phi = 0$  at the critical point of the phase separation. Note that Eq. (9) could be postulated in a phenomenological approach, since the relevant energy associated with the continuous phase transition is the decrease of the internal energy per unit volume when the mixture becomes phase separated,  $-dJ\Phi^2$ , where  $\Phi$  is the proper critical OP. Consistent with the assumption of the symmetrical mixture we postulate the lattice gas or ideal-mixing form for the entropy,

$$-Ts = k_B T \int_0^L dz \sum_{i=1}^4 \rho_i(z) \ln \rho_i(z). \quad (12)$$

When the total density is fixed (see (4)), there are three independent variables, and the natural choice is  $\rho_q$ ,  $\Phi$  and  $\rho_{ion}$  (see (8), (10) and (11)). We thus consider the grand

potential (3) as a functional of these three fields,  $\omega[\Phi, \rho_q, \rho_{ion}]$ . In the bulk  $\rho_q = 0$  due to the charge neutrality. We limit ourselves to the critical composition, and assume that in the bulk  $\Phi = 0$ . The bulk density of ions,  $\bar{\rho}_{ion}$ , is determined by  $T$  and the chemical potential from the condition  $\frac{\partial \omega[0, 0, \rho_{ion}]}{\partial \rho_{ion}} = 0$ , and can be chosen as the independent variable. From the minimum condition of  $\omega[\Phi, \rho_q, \rho_{ion}]$  with respect to  $\rho_{ion}(z)$  we can obtain  $\rho_{ion}(z)$  in terms of  $\Phi(z)$  and  $\rho_q(z)$  (see Appendix A), and  $\omega$  becomes a functional of two fields,  $\Phi(z)$  and  $\rho_q(z)$ . In order to calculate the effective interaction between the surfaces, we have to calculate the excess grand potential per surface area, and subtract the  $L$ -independent surface energies (surface tensions) at the two walls. We introduce the functional

$$\mathcal{L}[\Phi, \rho_q] = \omega[\Phi, \rho_q, \rho_{ion}] - \omega[0, 0, \bar{\rho}_{ion}]. \quad (13)$$

$\mathcal{L}$  is the sum of the effective interactions between the surfaces,  $\Psi(L)$ , and the  $L$ -independent surface energies. In the critical region (not too close to the surface) the fields are small, and the entropy (Eq. (12)) can be Taylor expanded in terms of  $\Phi$  and  $\rho_q$ . In the one-phase region the fourth order terms in the fields can be neglected, and we finally obtain the approximation (see Appendix A)

$$\beta \mathcal{L}[\Phi, \rho_q] \approx \int_0^L dz \left[ \frac{\bar{\beta}}{2} \left( \xi^{-2} \Phi^2 + (\nabla \Phi)^2 \right) - \frac{\rho_q^2 \Phi}{2 \bar{\rho}_{ion}} \right] + \beta \mathcal{L}_C^s + \beta \mathcal{L}_{DH}[\rho_q], \quad (14)$$

where  $\bar{T} = 1/\bar{\beta} = k_B T/J$  is the dimensionless temperature, in the mean-field approximation (MF) the critical temperature is  $\bar{T}_c = 2d$  and the bulk correlation length is  $\xi = (\bar{T} - \bar{T}_c)^{-1/2}$ ,

$$\beta \mathcal{L}_C^s = \bar{\beta} \left[ \frac{1}{2} \left( \Phi^2(0) + \Phi^2(L) \right) - h_0 \Phi(0) - h_L \Phi(L) \right] \quad (15)$$

is the contribution associated with the surfaces, and

$$\beta \mathcal{L}_{DH}[\rho_q] = \int_0^L dz \left[ \frac{1}{2 \bar{\rho}_{ion}} \rho_q^2 + \beta e \rho_q \psi - \frac{\beta \epsilon}{8\pi} (\nabla \psi)^2 \right] + \beta \left( e \sigma_0 \psi(0) + e \sigma_L \psi(L) \right). \quad (16)$$

The electrostatic potential  $\psi$  satisfies the Poisson equation (6) with the BC (7); for this reason  $\beta \mathcal{L}$  is a functional of only two independent fields.

Note that  $\frac{\rho_q^2(z)}{2 \bar{\rho}_{ion}}$  in Eq. (14) plays a role of a position-dependent external field acting on the OP  $\Phi$ . The physical origin of this “external field” is the excess number density of ions near the charged wall (it decays as  $\rho_q^2(z)$ ), and the preferential solubility of the ions in the phase with  $\Phi > 0$ .

Given the complexity of the considered system, the functional (14) has a rather simple form. At the same time it captures the essential physics of the near-critical mixture containing ions with preferential solubility in one of the mixture components. We believe that this functional can serve as a generic model of such systems. Very close to the critical point it is necessary to add terms  $\propto \Phi^4, \Phi^2 \rho_q^2$  to the integrand in Eq. (14), because  $\xi^{-1} \rightarrow 0$  for  $T \rightarrow T_c$ . This will be a subject of a separate study.

In equilibrium  $\Phi$  and  $\rho_q$  take the forms corresponding to the minimum of the functional (14). From  $\frac{\delta \mathcal{L}}{\delta \Phi} = 0$  we obtain the first Euler-Lagrange (EL) equation

$$\frac{d^2 \Phi(z)}{dz^2} = \xi^{-2} \Phi(z) - \frac{\bar{T} \rho_q^2(z)}{2 \bar{\rho}_{ion}}, \quad (17)$$

with the boundary conditions (see Refs. [30, 31], but note the difference in the definitions of the surface fields)

$$\Phi'(0) - \Phi(0) = -h_0, \quad \Phi'(L) + \Phi(L) = h_L, \quad (18)$$

and from  $\frac{\delta \mathcal{L}}{\delta \rho_q} = 0$  we obtain the second EL equation

$$e\psi(z) = -\frac{k_B T}{\bar{\rho}_{ion}} \rho_q(z) (1 - \Phi(z)). \quad (19)$$

In the more general case, i.e. without the assumption that the difference between the vdW interactions of water and ions is negligible [32], there are two differential EL equations instead of Eq. (17); one for the excess number density of ions and the other one for the excess solvent concentration. The present analysis is much simpler.

The nonlinear equations (17) and (19) can be solved numerically. However, when the term  $\propto \rho_q^2 \Phi$  in (14) is treated as a perturbation, we can obtain analytical results in the perturbation expansion, as we did in Ref. [32] for  $y \gg 1$ . In the next section we present the approximate analytical results for the shape of the OP profile and for the excess grand potential in the case of  $y < 1$ , and compare them with the numerical solutions of the full EL equations.

### III. APPROXIMATE SOLUTIONS OF THE EULER-LAGRANGE EQUATIONS

Let us first consider the linearized EL equations,

$$\frac{d^2 \Phi^{(1)}(z)}{dz^2} = \xi^{-2} \Phi^{(1)}(z), \quad (20)$$

and

$$e\psi^{(1)}(z) = -\frac{k_B T}{\bar{\rho}_{ion}} \rho_q^{(1)}(z). \quad (21)$$

The Poisson equation and Eq. (21) give

$$\frac{d^2}{dz^2} \rho_q^{(1)}(z) = \kappa^2 \rho_q^{(1)}(z), \quad (22)$$

with

$$\kappa = \sqrt{\frac{4\pi e^2 \bar{\rho}_{ion}}{k_B T \epsilon}}. \quad (23)$$

In Ref. [32] the second term in Eq. (17) was neglected, and  $\Phi$  was approximated by  $\Phi^{(1)}$ . Thus, only the effect of the critical adsorption on the charge distribution was taken into account for  $y > 1$ .

As shown in the case of weak surface fields in ion-free systems, the shape of the OP profile can have a strong effect on the Casimir potential [19, 21]. It is thus important to determine how the near-surface composition  $\Phi(z)$  is influenced by the charge distribution  $\rho_q(z)$ , and next how the modified shape of  $\Phi(z)$  influences the Casimir potential. In this section we focus on this question for  $y < 1$ . We should note that for  $y < 1$  the bulk correlation length is shorter than the screening length, and the system may be at the crossover between MF and the universal critical regime. In this work we shall limit ourselves to the MF approximation. Preliminary results for surfaces with opposite adsorption preferences were presented in Ref. [31].

We assume that the surface fields and the surface charge-densities are small and of the same order of magnitude. Thus, the values of  $\rho_q$  and  $\Phi$  are small and comparable, and we can assume that  $\Phi - \Phi^{(1)}, \rho_q - \rho_q^{(1)} = O(\rho_q^{(1)2}, \Phi^{(1)2})$ . In such a case  $\rho_q^2 \Phi$  in (14) can be treated as a perturbation, and Eqs. (17) and (19) can be approximated by

$$\frac{d^2 \Phi(z)}{dz^2} = \xi^{-2} \Phi(z) - \frac{\bar{T} \rho_q^{(1)2}(z)}{2 \bar{\rho}_{ion}}, \quad (24)$$

and

$$e\psi(z) = -\frac{k_B T}{\bar{\rho}_{ion}} (\rho_q(z) - \rho_q^{(1)}(z) \Phi^{(1)}(z)). \quad (25)$$

The shapes of  $\Phi(z)$  obtained from (24) in a semiinfinite system and in a slit are discussed in Secs. IIIA and IIIB respectively.

### A. OP profiles near a single wall

In the semiinfinite system the well-known solutions of (22) and (20) are

$$\rho_q^{(1)}(z) = -\kappa\sigma_0 e^{-\kappa z}, \quad (26)$$

and

$$\Phi^{(1)}(z) = \frac{h_0}{1 + \xi^{-1}} e^{-z/\xi}. \quad (27)$$

We insert (26) in Eq. (24), and from the boundary condition (18) obtain

$$\Phi(z) = \frac{H_0}{1 + \xi^{-1}} e^{-z/\xi} - B\sigma_0^2 e^{-2\kappa z}, \quad (28)$$

where

$$H_0 = \left[ h_0 + (1 + 2\kappa)B\sigma_0^2 \right], \quad (29)$$

and

$$B = \frac{\bar{T}y^2}{2\bar{\rho}_{ion}(4y^2 - 1)} \approx \frac{3y^2}{\bar{\rho}_{ion}(4y^2 - 1)}. \quad (30)$$

The last equality in (30) is valid for  $\bar{T} \approx \bar{T}_c$ . Eqs.(28)-(30) are valid for  $z \gtrsim \xi, 1/\kappa$ , due to the assumptions made in derivation of the coarse-grained description.

Note that the effect of the charges on the OP profile is twofold. First, the surface field  $h_0$  is renormalized, and the renormalized  $H_0$  depends on  $h_0$  and on  $\sigma_0, \bar{\rho}_{ion}, \kappa$  and  $\xi$ . The surface field has a microscopic range, and the first contribution to the excess OP  $\Phi(z)$  is a result of the critical correlations. The additional term in Eq. (28) has the same decay length as the “external field”,  $\rho_q^{(1)2}(z)$ .

For  $y < 1/2$  the asymptotic decay of  $\Phi(z)$  at large  $z$  is determined by the second term in (28). In such a case  $\Phi(z) > 0$  for large  $z$  for both hydrophilic and hydrophobic surfaces, since  $-B > 0$  for  $y < 1/2$ . Moreover, it depends only on  $\sigma_0$ . This is because for  $\xi < z < 1/2\kappa$  the effect of the surface selectivity is negligible, but near the wall there is an excess number density of ions, and ions are soluble in water.

For  $y > 1/2$  the first term in (28) determines the behavior at large  $z$ . In the case of hydrophilic surfaces (with  $h_0 > 0$ )  $|H_0| > |h_0|$ . In the case of hydrophobic surfaces either  $|H_0| < |h_0|$ , or the effective surface field changes sign,  $H_0 > 0$ . The prefactor  $H_0$  can be positive in the case of a hydrophobic surface when the surface charge is large, because  $B > 0$  for  $y > 1/2$ .

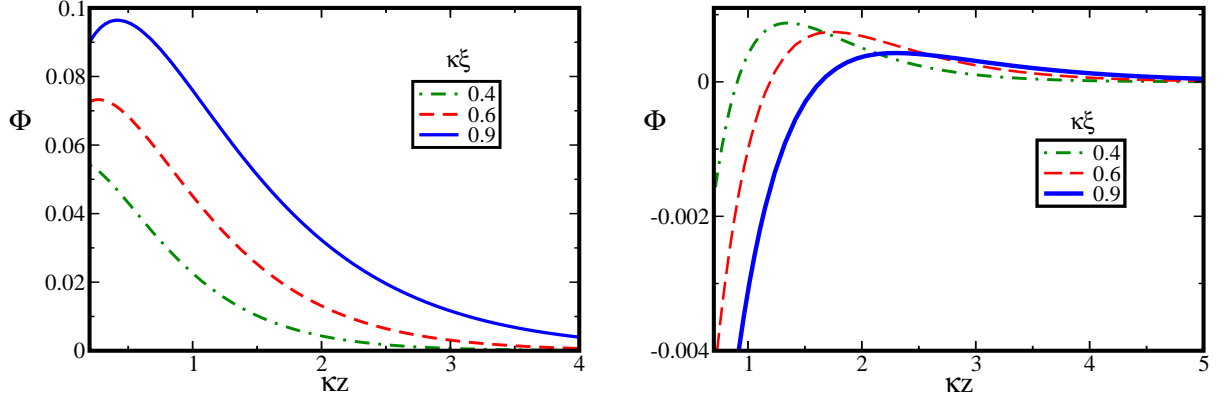


FIG. 1: The OP (excess concentration) in the semiinfinite system defined in Eq. (10) and approximated by Eq. (28). The dimensionless number density of ions, the inverse screening length and the surface field are  $\bar{\rho}_{ion} = 10^{-3}$ ,  $\kappa = 0.1$  and  $|h_0| = 0.05$  respectively (the length unit is the molecular size  $a$ ). (Left) The wall is hydrophilic and the charge density is  $\sigma_0 = 0.016$ . (Right) The wall is hydrophobic and the charge density is  $\sigma_0 = 0.007$ .

In order to understand the physical reason for changing the weakly hydrophobic surface into effectively hydrophilic one, recall that the charged surface attracts oppositely charged ions. As a result of the entropy of mixing, excess of like charged ions near the surface is also present. The excess of water-soluble ions acts as an external field for the OP (see the last term in the integrand in Eq. (14)). This 'external field' enhances the effect of the surface field  $h_0$  in the case of the hydrophilic surface, and competes with  $h_0$  in the case of the hydrophobic surface. If the 'external field' is much stronger than the selectivity of the surface due to the short-range wall-fluid interactions, then excess of water can occur near the hydrophobic surface. We discuss in more detail in what conditions  $\Phi(z)$  is nonmonotonic in Appendix B.

Note that  $B \rightarrow \infty$  for  $y \rightarrow 1/2$ . However, for  $y = 1/2$  the decay rates of the two terms in (28) are the same, and the singularities in (28) cancel against each other. Assuming  $\xi, z \gg 1$  and  $\bar{T} \approx \bar{T}_c = 6$  we obtain for  $y = 1/2$

$$\Phi(z) = h_0 \left[ 1 + \alpha_0 \frac{z}{\xi} \right] e^{-z/\xi}, \quad (31)$$

where  $\alpha_0 = \frac{3\sigma_0^2}{8\bar{\rho}_{ion}h_0}$ . When  $\alpha_0 > 1$  or  $\alpha_0 < 0$  then the profile (31) is nonmonotonic. Characteristic OP profiles near the hydrophilic and the hydrophobic surface are shown in Fig. 1.

Nonmonotonic OP profile has been obtained previously in charge-neutral critical systems

in the case of weak surface fields [18, 19, 21, 38] as a result of correlations between critical fluctuations. In our case the RHS in Eq. (17) can be negative when the 'external field'  $\rho_q(z)^2$  is sufficiently large compared to  $\Phi(z)$ . As a result, a maximum of  $\Phi(z)$  can be present when  $h_0$  is small compared to  $\sigma_0$ , in some analogy to the weak surface fields in neutral systems. Note that the surface field is 'strong' or 'weak' in comparison with the surface charge.

## B. OP profiles in a slit

In the slit the solution of the linearized EL equation for the charge distribution is (see (21), (6), (7))

$$\rho_q^{(1)}(z) = \frac{-\kappa}{S} \left[ S_0 e^{-\kappa z} + S_L e^{-\kappa(L-z)} \right]. \quad (32)$$

The coefficients in Eq. (32) and the explicit expression for the solution of Eqs. (25) and (6) with the Neumann BC (7) for  $\rho_q(z)$ , are given in Appendix C.

The solution  $\Phi^{(1)}(z)$  of the linearized EL equation (20) with the BC (18) has the form

$$\Phi^{(1)}(z) = n_0 e^{-z/\xi} + n_L e^{-(L-z)/\xi}, \quad (33)$$

with the coefficients given in Appendix D. Finally, the solution of Eq. (24) with  $\rho_q^{(1)}(z)$  given in Eq. (32), and with the boundary conditions (18) is

$$\Phi(z) = A_0(L) e^{-z/\xi} + A_L(L) e^{-(L-z)/\xi} - S_0^2 Q(L) e^{-2\kappa z} - S_L^2 Q(L) e^{-2\kappa(L-z)} + S_0 S_L C e^{-\kappa L}, \quad (34)$$

with the coefficients given in Appendix D. In Fig. 2 we show the profiles in a slit with identical hydrophilic surfaces for fixed temperature and surface properties, for weak (left plot) and strong (right plot) surface charge and for different widths of the slit. In Fig. 3 analogous profiles are shown for identical hydrophobic surfaces.

In Fig. 4 we show the concentration profiles for strongly selective and weakly charged left surface, and weakly selective and strongly charged right surface. The strongly charged weakly selective surface (either hydrophilic or hydrophobic) acts as an effectively hydrophilic one because of relatively large concentration of inorganic ions near the surface, and preferential solubility of the ions in water (see the cartoon in Fig. 5). As we show in the next subsection, this fact can lead to a different sign of the Casimir potential than predicted by Eq. (1).

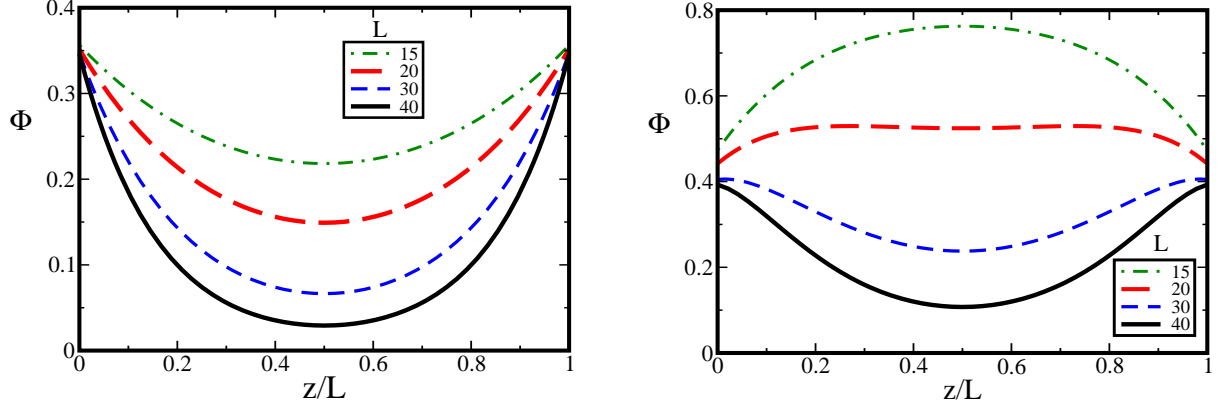


FIG. 2: The OP (excess concentration) in a slit defined in Eq. (10) and approximated by Eq. (34). The identical walls are hydrophilic. The dimensionless surface field, number density of ions, the inverse screening length and the correlation length are  $h_0 = 0.4$ ,  $\bar{\rho}_{ion} = 10^{-3}$ ,  $\kappa = 0.1$  and  $\xi = 6$ , respectively. (Left) Weak surface charge,  $\sigma_0 = 0.006$ . (Right) Strong surface charge,  $\sigma_0 = 0.025$ . From the top to the bottom line the width of the slit is  $L = 15, 20, 30, 40$ . The length unit is the molecular size  $a$ .

We can summarize that the charged hydrophilic surface acts as even more hydrophilic, whereas the charged hydrophobic surface becomes less hydrophobic, and can lead even to excess of water if the surface charge is large and ions are soluble in water.

#### IV. THE EFFECTIVE POTENTIAL

We have shown that the presence of hydrophilic ions near the selective surfaces can lead to significant qualitative modifications of the concentration profile in the slit (Figs.2-4). In this section we determine the effect of these modifications of the OP on the effective interactions between the surfaces. In the approximation consistent with (24) the excess grand potential takes the form

$$\beta\mathcal{L} \approx \int_0^L dz \left[ \frac{\bar{\beta}}{2} \left( \xi^{-2} \Phi^2 + (\nabla \Phi)^2 \right) - \frac{\rho_q^{(1)2} \Phi}{2\bar{\rho}_{ion}} \right] + \beta\mathcal{L}_C^s + \beta\mathcal{L}_{DH}[\rho_q] \quad (35)$$

where  $\beta\mathcal{L}_C^s$  and  $\beta\mathcal{L}_{DH}[\rho_q]$  are given in Eqs.(15) and (16). In thermodynamic equilibrium  $\rho_q^{(1)}$ ,  $\Phi$ ,  $\rho_q$  and  $\psi$  satisfy Eqs.(22), (24), (25) and (6) respectively. Using the above equations and the BC (7), (18), integrating by parts and approximating  $\rho_q^{(1)2} \Phi$  by  $\rho_q^{(1)2} \Phi^{(1)}$  we obtain

$$\beta\mathcal{L} \approx \frac{1}{4\bar{\rho}_{ion}} \int_0^L dz \rho_q^{(1)2}(z) \Phi^{(1)}(z) + \frac{\beta}{2} \left( \sigma_0 \psi(0) + \sigma_L \psi(L) \right) - \frac{\bar{\beta}}{2} \left( h_0 \Phi(0) + h_L \Phi(L) \right). \quad (36)$$



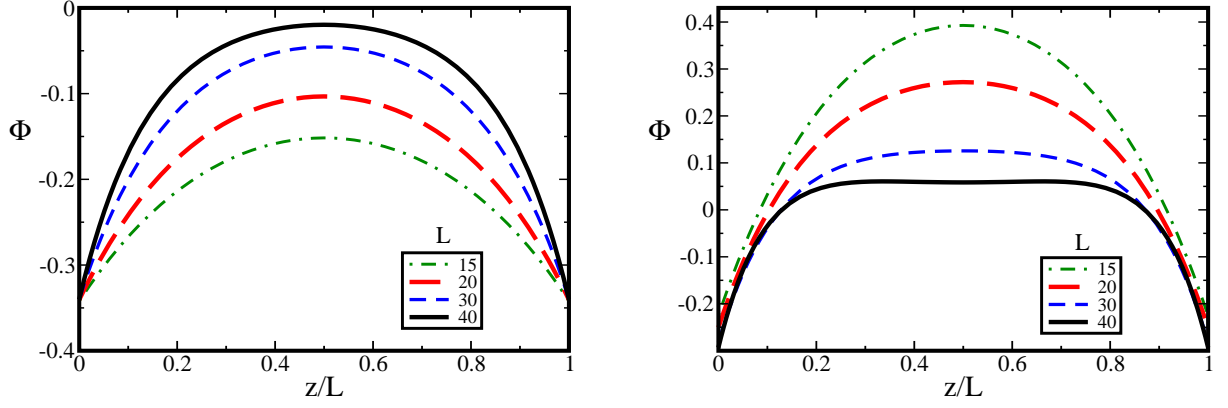


FIG. 3: The OP (excess concentration) in a slit defined in Eq. (10) and approximated by Eq. (34). The identical walls are hydrophobic. The dimensionless surface field, number density of ions, the inverse screening length and the correlation length are  $h_0 = -0.4$ ,  $\bar{\rho}_{ion} = 10^{-3}$ ,  $\kappa = 0.1$  and  $\xi = 6$  respectively. (Left) Weak surface charge,  $\sigma_0 = 0.006$ . From the bottom to the top line the width of the slit is  $L = 15, 20, 30, 40$ . (Right) Strong surface charge,  $\sigma_0 = 0.025$ . From the top to the bottom line the width of the slit is  $L = 15, 20, 30, 40$ . The length unit is the molecular size  $a$ .

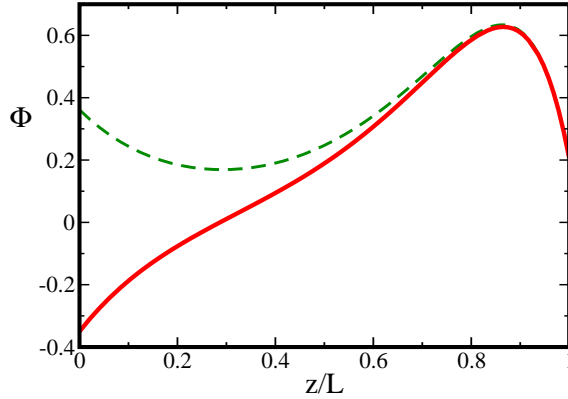


FIG. 4: The OP (excess concentration) in a slit defined in Eq. (10) and approximated by Eq. (34). One surface is strongly selective and weakly charged, whereas the other surface is weakly selective and strongly charged. The dimensionless surface fields, surface charge densities, number density of ions, the inverse screening length, the correlation length and the width of the slit are  $|h_0| = 0.4$ ,  $|h_L| = 0.001$ ,  $\sigma_0 = 0.001$ ,  $\sigma_L = 0.05$ ,  $\bar{\rho}_{ion} = 10^{-3}$ ,  $\kappa = 0.1$ ,  $\xi = 8$  and  $L = 30$  (the length unit is the molecular size  $a$ ). The left wall is hydrophobic (solid line), or hydrophilic (dashed line). The curves for weakly hydrophilic or weakly hydrophobic right wall are almost the same, and are indistinguishable on the plot.

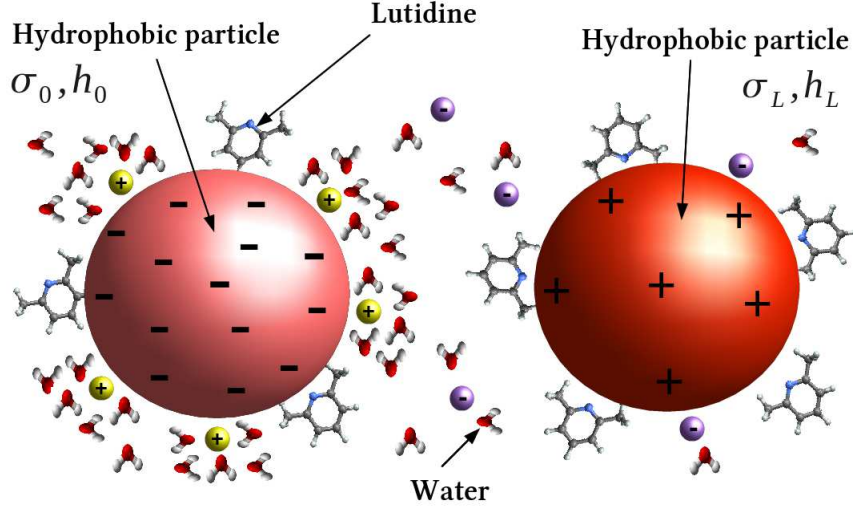


FIG. 5: Schematic representation of the distribution of the components in the case of colloid particles. Repulsion can appear between surfaces with opposite charges and like selectivity when  $\sigma_0 \gg \sigma_L$  and  $h_0 \ll h_L$  and the Debye length is bigger than the correlation length. The theory has been developed for a slit geometry. The distribution of the components and the interaction between curved surfaces of the colloid particles, however, have the same qualitative features and can be obtained by using the Derjaguin approximation [32].

In the critical region and for weak ionic strength  $\xi, 1/\kappa \gg 1$ , so we can make the approximations  $1 + \xi^{-1} \approx 1$ ,  $1 + \kappa \approx 1$ . We use (32), (34) and Appendix C, subtract the surface tension contributions, assume the MF result  $\bar{\beta} \approx 1/6$  for the near-critical temperature, and finally obtain the explicit asymptotic expression for the effective interactions (per microscopic area  $a^2$ ) for  $y < 1$ ,

$$\beta\Psi(L) \approx -\frac{A_\xi}{\xi}e^{-L/\xi} + \frac{\kappa A_\kappa}{\bar{\rho}_{ion}}e^{-\kappa L} + \frac{\kappa A_{2\kappa}}{\bar{\rho}_{ion}}e^{-2\kappa L} \quad (37)$$

where the terms that decay faster are neglected,

$$A_\xi = \frac{2h_0h_L}{\bar{T}} + \frac{y^2(\sigma_0^2h_L + \sigma_L^2h_0)}{\bar{\rho}_{ion}(4y^2 - 1)} \quad (38)$$

and

$$A_\kappa = 2\sigma_0\sigma_L - \frac{2y(1+y)\sigma_0\sigma_L(h_0 + h_L)}{(2y + 1)}. \quad (39)$$

The above two amplitudes agree precisely with the corresponding amplitudes obtained in Ref.[32] (note the different definitions of the surface fields here and in Ref.[32]). For  $y < 1$ , however,  $e^{-2\kappa L} > e^{-L/\xi}e^{-\kappa L}$ , and instead of the term  $\propto e^{-L/\xi}e^{-\kappa L}$  taken into account in Ref.[32] for  $y > 1$ , we include in (37) the term  $\propto e^{-2\kappa L}$ . The corresponding amplitude is

$$A_{2\kappa} = \left[ (\sigma_0^2 + \sigma_L^2) - (\sigma_0^2 h_0 + \sigma_L^2 h_L) \left( \frac{2y(y+1)}{2y+1} \right) - (\sigma_0^2 h_L + \sigma_L^2 h_0) \left( \frac{y(4y^2-2)}{4y^2-1} \right) \right]. \quad (40)$$

For  $y < 1$  it is necessary to include the last term in Eq. (37) in order to correctly describe the distances  $L \simeq 1/2\kappa$  even on the level of the linearized EL equations. In the DH theory for nonadsorbing surfaces ( $h_0 = h_L = 0$ ) the amplitude simplifies to  $A_{2\kappa} = \sigma_0^2 + \sigma_L^2$ .

The first term in (38) is the MF Casimir amplitude, and the first terms in (39) and (40) are the amplitudes in the effective electrostatic potential between the surfaces in the DH theory. The effective potential can be approximated by (1) supplemented with the term  $\frac{\kappa(\sigma_0^2 + \sigma_L^2)}{\bar{\rho}_{ion}} \exp(-2\kappa L)$  when the correction terms in (38)-(40) are negligible. However, the correction and the leading-order terms in  $A_\xi$  are comparable if either  $\sigma_0^2/\bar{\rho}_{ion}$  is comparable with  $h_0$ , or  $\sigma_L^2/\bar{\rho}_{ion}$  is comparable with  $h_L$ . Recall that in such a case the OP profile (28) is nonmonotonic near the respective wall (see Appendix B). Thus, we can expect significant deviation from the MF Casimir amplitude when the surface charges lead to a qualitative change of  $\Phi(z)$ . This is analogous to the nonuniversal Casimir potential in the case of weak surface fields leading to nonmonotonic OP profile in charge-neutral systems [19, 21].

The amplitude  $|A_\kappa|$  that governs the large-distance decay of  $\beta\Psi(L)$  (see (39)) is smaller for hydrophilic surfaces ( $h_0, h_L > 0$ ) than for hydrophobic surfaces ( $h_0, h_L < 0$ ). Thus the screening of the hydrophilic surface by hydrophilic ions is better than screening of the hydrophobic surface. In addition, from (38) we can see that  $A_\xi$  is larger for hydrophilic surfaces than for hydrophobic surfaces. This is because the presence of hydrophilic ions enhances the hydrophilicity of the hydrophilic surface, and competes with the hydrophobicity of the hydrophobic surface. Thus, the hydrophilic ions lead to opposite changes of the effective potential for hydrophilic and hydrophobic surfaces.

Terms of higher order in the surface charges and the surface fields are neglected in (38)-(40). For large differences between the fields some of the neglected terms can be relevant, therefore for different orders of magnitude of  $\sigma_0$ ,  $\sigma_L$  and  $h_0$ ,  $h_L$  our results can deviate from the exact solution on a quantitative level. We discuss this issue in Sec.V.

The correction terms in both  $A_\xi$  and  $A_{2\kappa}$  diverge for  $y = 1/2$ . However, for  $y = 1/2$  the

decay rates  $\xi$  and  $1/2\kappa$  are the same, and the divergent terms cancel against each other. For  $y = 1/2$  we obtain from (37)

$$\beta\Psi(L) \approx \frac{\kappa A_\kappa}{\bar{\rho}_{ion}} e^{-\kappa L} + \frac{\kappa B_{2\kappa}(L)}{\bar{\rho}_{ion}} e^{-2\kappa L} \quad (41)$$

with finite coefficients given in Appendix E.

### A. Identical surfaces

Let us discuss in more detail the case of two identical surfaces,  $h_0 = h_L$ ,  $\sigma_0 = \sigma_L$ , relevant for interactions between identical colloidal particles. In the special case of  $y = 1/2$  and  $h_0 = h_L$ ,  $\sigma_0 = \sigma_L$  the amplitudes in Eq. (41) are

$$A_\kappa = \sigma_0^2 \left( 2 - \frac{3}{2} h_0 \right) \quad (42)$$

and

$$B_{2\kappa}(L) = 2\sigma_0^2 - \frac{4\bar{\rho}_{ion}h_0^2}{\bar{T}} - \frac{h_0\sigma_0^2}{2}(3 + 2\kappa L). \quad (43)$$

$A_\kappa > 0$  for weak surface fields to which analytical expressions are restricted. Thus, the repulsion dominates at large distances.

At shorter distances, the form of  $\Psi(L)$  depends on the sign and magnitude of  $B_{2\kappa}(L)$ . The Casimir attraction competes with the electrostatic repulsion in the first two terms in (43). The correction term in (43) is negative for hydrophilic and positive for hydrophobic surfaces. From (43) it follows that the surface charge must be smaller for hydrophobic than for hydrophilic surfaces to overcome the electrostatic repulsion and obtain attraction at short distances. Similar behavior is found for  $y \neq 1/2$ , as shown in Fig. 6. In the lowest-order approximation (1) the effective potential is the same between two hydrophobic surfaces and between two hydrophilic surfaces if the surface charges and the absolute values of the surface fields are the same. The coupling between the concentration and the charge distributions can lead to qualitative differences of the effective interactions between two hydrophobic or two hydrophilic surfaces with the same values of  $\sigma_0$  and  $|h_0|$ .

In Fig. 7 we demonstrate the sensitivity of  $\Psi(L)$  to the surface charge. For weak surface charge (left panel) we can see a crossover from the SALR type potential (attraction at short and repulsion at large distances) for  $\xi = 4$  (green dashed-dotted line) to the attractive

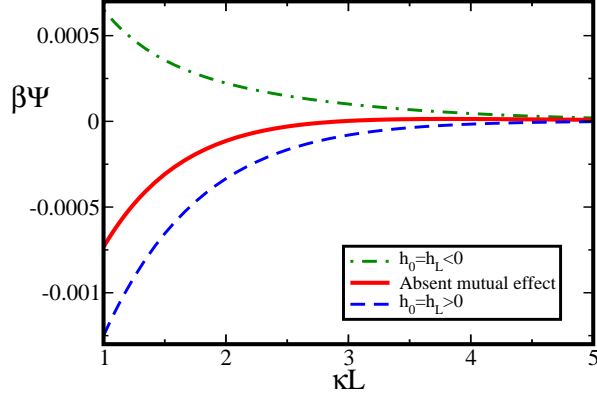


FIG. 6: The effective potential per microscopic area in  $k_B T/a^2$  units, Eq. (41), for the dimensionless surface charge  $\sigma_0 = \sigma_L = 0.004$ , number density of ions  $\bar{\rho}_{ion} = 0.001$  and the dimensionless surface field  $|h_0| = |h_L| = 0.4$ . The inverse Debye length is  $\kappa = 0.1$  and the correlation length is  $\xi = 8$ ; length is in units of the microscopic size  $a$ . The effect of the charge distribution on the critical adsorption is neglected for the solid line. Dashed and dash-dotted lines represent the

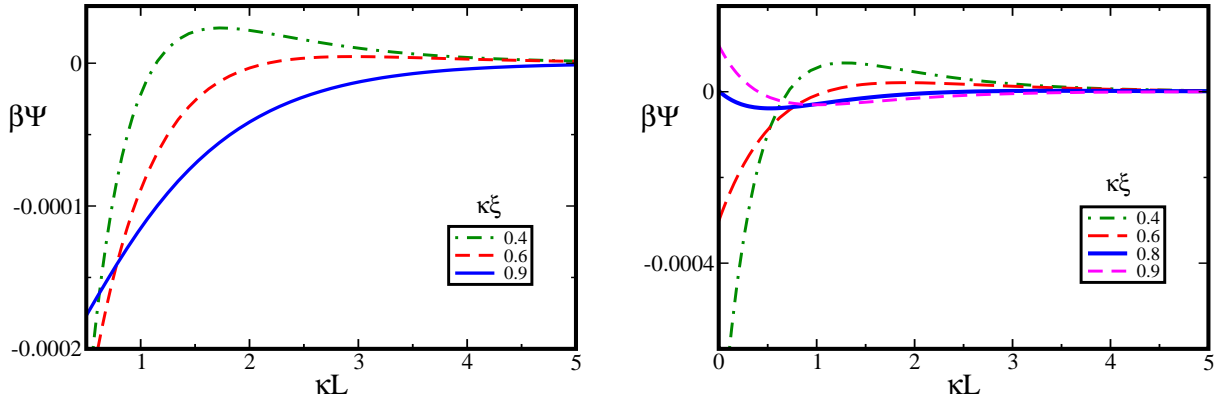


FIG. 7: The effective potential per microscopic area in  $k_B T/a^2$  units, Eq. (41), between identical hydrophobic walls with  $h_0 = -0.14$ ,  $\kappa = 0.1$ , and the dimensionless number density of ions  $\bar{\rho}_{ion} = 0.001$ . (Left)  $\sigma_0 = 0.001$ . (Right)  $\sigma_0 = 0.0013$ .

potential for  $\xi = 9$  (solid blue line). For stronger surface charge (right panel), the potential far away from  $T_c$  is repulsive at large separations, and assumes a maximum for smaller separation between the surfaces. On approaching  $T_c$  the maximum changes to a minimum.

## B. Significant deviations from Eq. (1)

Here we focus on the question for what surface properties the effective potential can deviate significantly from Eq. (1). The electrostatic repulsion is proportional to  $\sigma_0\sigma_L$ , and is weak when the surface charge at one surface is small. The MF Casimir amplitude is proportional to  $h_0h_L$ , and is weak when one of the surface fields is small. We thus need to find such surface charges and surface fields for which one of the correction terms in (38) - (39) is larger than both  $\sigma_0\sigma_L/\bar{\rho}_{ion}$  and  $h_0h_L$ . This is possible when the strongly selective surface is weakly charged, and the weakly selective one is strongly charged ( $\sigma_L \gg \sigma_0$  and  $h_L \ll h_0$ ). In such a case the term  $\sigma_L^2 h_0/\bar{\rho}_{ion}$  can dominate.

We focus on  $y = 1/2$  where the analysis is simpler. When  $\sigma_0 h_L \ll \sigma_L$  and  $\sigma_0^2 \ll h_0$ , then the term with the largest amplitude is (see Appendix E)

$$\beta\Psi(L) \simeq -\frac{\sigma_L^2 h_0}{2}\kappa L e^{-2\kappa L}. \quad (44)$$

Attraction and repulsion is expected for  $h_0 > 0$  and  $h_0 < 0$  respectively. The potential (37) is shown in Fig. 8 (left) and Fig. 8 (right) for like and opposite surface charges respectively. The corresponding OP profiles are shown in Fig. 4.

Note that when both the Casimir and the electrostatic potentials are *repulsive*, *attraction* at intermediate distances, followed by a small repulsion barrier occurs when one surface is strongly hydrophilic and weakly charged, and the other one is weakly hydrophobic and strongly charged. Such phenomenon was observed experimentally between a colloid particle and a substrate in Ref.[6]. When the Casimir and the DH potential are *both attractive*, the potential between two oppositely charged hydrophobic surfaces can be *repulsive* at intermediate distances, and very weakly attractive at larger distances (see the cartoon in Fig. 5). This may happen when one of the two surfaces is strongly hydrophobic and weakly charged, and the other one is weakly hydrophobic and strongly charged. In such a case the second surface behaves as a hydrophilic one (see Fig. 4 and 8), and in the case of weak electrostatic attraction the Casimir repulsion can dominate.

When the surface charge and selectivity of the two confining surfaces are both much different, then the total potential can be qualitatively different than in Eq. (1). Attraction can be present when both terms in (1) are repulsive, and repulsion can be present when both terms in (1) are attractive. The strongly hydrophilic and hydrophobic surfaces show *opposite*

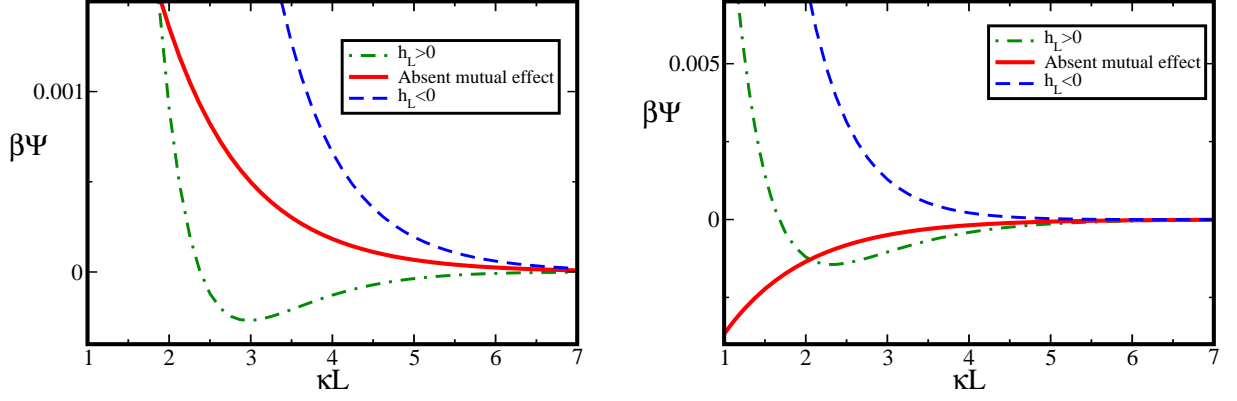


FIG. 8: The effective potential  $\beta\Psi(L)$  per microscopic area in  $k_B T/a^2$  units, given by Eq. (1) (central curves) and by Eq. (37) (top and bottom curves) for strong selectivity and small surface charge at one surface and weak selectivity and large surface charge at the other surface. The dimensionless density of ions is  $\bar{\rho}_{ion} = 0.001$ , the correlation length is  $\xi = 8$  and the inverse screening length is  $\kappa = 0.1$ . The length unit is the molecular size  $a$ . (Left)  $\sigma_0 = 0.05$  and  $\sigma_L = 0.001$  and (Right)  $\sigma_0 = 0.05$  and  $\sigma_L = -0.001$ , and the dimensionless surface fields are  $h_L = 0.4$  and  $h_0 = \pm 0.001$  (central and bottom curves), and  $h_L = -0.4$ ,  $h_0 = \pm 0.001$  (top curves). The curves with  $h_0 = 0.001$  and  $h_0 = -0.001$  cannot be distinguished on the plot.

trends. The strongly hydrophilic surface always leads to more attractive, and the strongly hydrophobic one always leads to more repulsive potential if the surfaces are charged.

## V. COMPARISON OF THE APPROXIMATE ANALYTICAL EXPRESSIONS WITH NUMERICAL SOLUTIONS OF THE FULL EL EQUATIONS

The main result of this work, Eqs.(37)-(40), was obtained under numerous assumptions and approximations. We assumed that the system is near the critical point and the concentration of ions is small, so that the correlation and the screening lengths are both much larger than the molecular size. Next we assumed that the dimensionless surface charges and surface fields are comparable and small. This assumption allows to truncate the expansion of the entropy in terms of  $\rho_q$  and  $\Phi$  at the lowest-order nontrivial term. However, for very large differences between the surface charges and the surface fields, as well as very close to the critical point where  $\xi^{-2} \rightarrow 0$ , the neglected contributions to the entropy become relevant. In this case the approximate expression may deviate from the exact result obtained by the

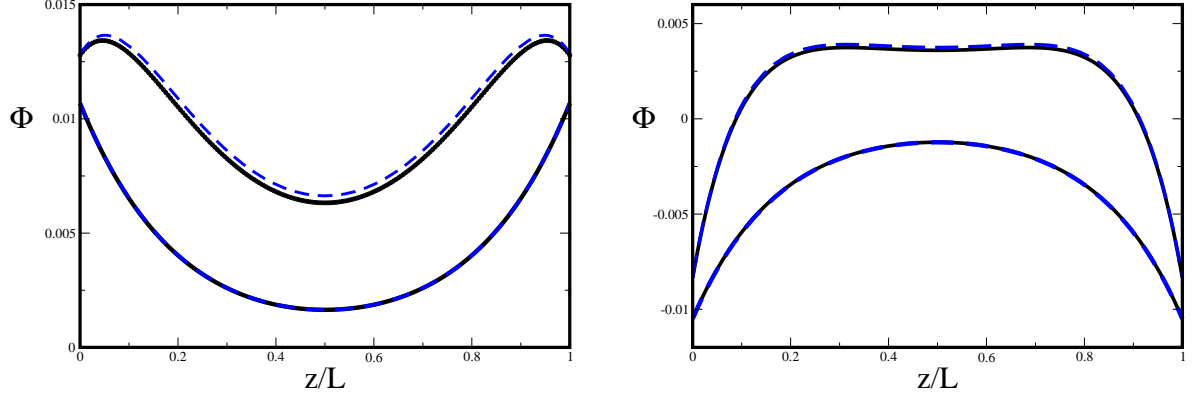


FIG. 9: The OP profiles for (Left) hydrophilic surfaces and (Right) hydrophobic surfaces with the dimensionless surface fields  $h_0 = h_L = \pm 0.012$  and dimensionless surface charge density  $\sigma_0 = \sigma_L = 0.005$  (top curves), and  $\sigma_0 = \sigma_L = 0.001$  (bottom curves). The dimensionless density of ions is  $\bar{\rho}_{ion} = 0.001$ , the inverse screening length is  $\kappa = 0.1$  and  $y = 0.745$ . The length unit is the molecular size  $a$ . Dashed-Lines represent Eq. (34) and solid lines represent numerical solutions of the full EL equations.

solutions of the full EL equations, (6) and (50)-(52).

In this subsection we check the validity of Eqs.(37)-(40) for various conditions. We solve numerically Eqs.(6) and (50)-(52) with the help of the package "bvpSolve". bvpSolve numerically solves boundary value problems (BVP) of ordinary differential equations (ODE). There are three methods of solving ODE in this package. For our purpose we choose "bvptwp" which is a mono-implicit Runge-Kutta (MIRK) method with deferred corrections by using conditioning in the mesh selection. In addition, we solve numerically Eqs.(6), (17) and (19). In the latter case we consider the approximate functional (14), but do not make further approximations for its EL equations. In Figs.9 and 10 we plot the numerical and the approximate analytical results for the OP profile (34) and for the effective potential (37) respectively for comparable surface charges and surface fields. As expected, good quantitative agreement is obtained when all the assumptions made in derivations of the approximate expressions are satisfied.

For significant differences between the surface charges and the surface fields the approximate expressions deviate from the numerical results, as shown in Fig. 11, and only semi-quantitative agreement is obtained. Nevertheless, we are convinced that the essential physics behind the strong mutual effects of the ions and critical adsorption, especially attraction



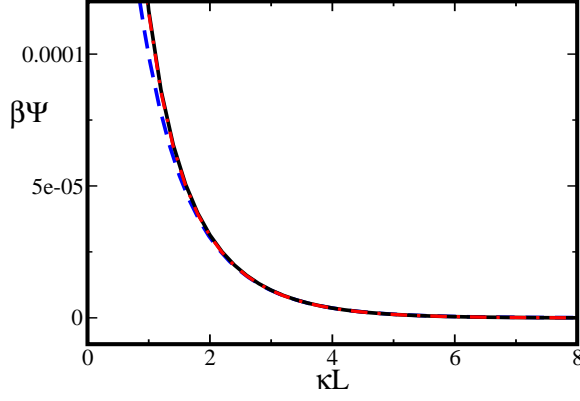


FIG. 10: The effective potential per microscopic area,  $\beta\Psi/a^2$ , where  $a$  is the molecular size. The dimensionless surface fields are  $h_0 = h_L = 0.006$  and the dimensionless surface charge density is  $\sigma_0 = \sigma_L = 0.001$ . The dimensionless density of ions is  $\bar{\rho}_{ion} = 0.001$ , the inverse screening length is  $\kappa = 0.1$  and  $y = 0.645$ . The length unit is the molecular size  $a$ . The dashed line is Eq. (37), the dashed-dot line is numerical solution to the approximate EL equations (Eqs.(6), (17) and (19)), and the solid line is the numerical solution to the full EL equations (Eqs.(6) and (50)-(52)).

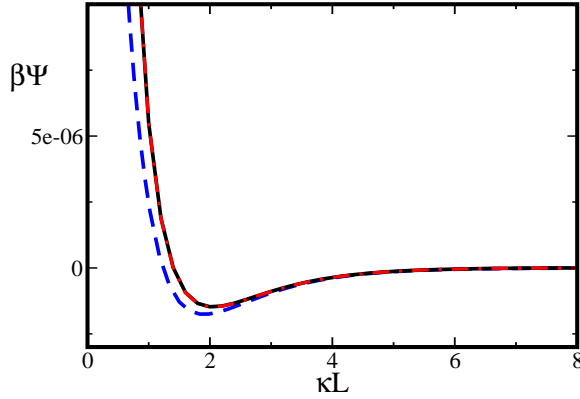


FIG. 11: The effective potential per elementary area,  $\beta\Psi/a^2$ , where  $a$  is the molecular size. The dimensionless surface fields are  $h_0 = -0.04$ ,  $h_L = -0.01$  and the dimensionless surface charge density is  $\sigma_0 = 0.001$  and  $\sigma_L = -0.0001$ . The dimensionless density of ions is  $\bar{\rho}_{ion} = 0.001$ , the inverse screening length is  $\kappa = 0.1$  and  $y = 0.645$ . The length unit is the molecular size  $a$ . The dashed line is Eq. (37), the dashed-dot line is numerical solution to the approximate EL equations (Eqs.(6), (17) and (19)), and the solid line is the numerical solution to the full EL equations (Eqs.(6) and (50)-(52)).

when both terms in (1) are repulsive and repulsion when both terms in (1) are attractive, is captured by our formulas (37)-(40).

## VI. SUMMARY

We have developed a new version of the Landau-type functional for confined near-critical binary mixture with ions. The new functional (see Eq. (14) -(16)) depends only on two fields - the charge density  $\rho_q(z)$  and the concentration difference between inorganic and organic components,  $\Phi(z)$ . In standard experiments the inorganic components are water and dissociating salt such as KBr. By minimizing the functional we obtained Euler-Lagrange equations, and next considered their approximate version (see (24) and (25)) that can be solved analytically. Unlike in Ref.[32], we focused on the case where the Debye screening length is larger than the correlation length of critical fluctuations. For such ratio  $y = \xi\kappa < 1$  of the relevant length scales the mutual effects of the charge distribution and the critical adsorption lead to strong violation of Eq. (1).

The analytical expression for  $\Phi(z)$  allows to determine the effect of charges on the distribution of the components between selective and charged surfaces. By considering first a semiinfinite system we have found that the key factor that determines the shape of  $\Phi$  is the ratio between  $\sigma_0^2/\bar{\rho}_{ion}$ , where  $\sigma_0$  is the surface charge and  $\bar{\rho}_{ion}$  is the bulk density of ions, and the surface selectivity  $|h_0|$ . If this ratio is large, then  $\Phi(z)$  can be nonmonotonic, and in the case of the hydrophobic surface even  $\Phi(z) > 0$ , indicating excess of water near the weakly hydrophobic surface. The reason for this behavior is the large amount of hydrophilic ions near the strongly charged surface. Preferential solubility of the ions in water dominates in this case over the weak hydrophobicity of the surface. This effectively hydrophilic behavior can lead to a different sign of the effective interactions than predicted by (1).

In the case of a slit with identical surfaces the shape of  $\Phi(z)$  can be qualitatively different from two extrema at  $z = 0$  and  $z = L$  expected for charge-neutral surfaces. A single maximum at  $z = L/2$  can be present between hydrophilic surfaces in narrow slits, as found before for weak surface fields in charge-neutral systems [19]. In the case of hydrophobic surfaces excess of water can occur in the center of the slit. These strong effects of the charges again occur when the ratio between  $\sigma_0^2/\bar{\rho}_{ion}$  and  $|h_0|$  is large.

The modification of the shape of  $\Phi(z)$  has the strongest consequence for the effective in-

teractions between the surfaces when one of them is strongly selective and weakly charged, and the other one is weakly selective and strongly charged. The first surface behaves as the charge-neutral one, whereas at the second surface the profile is nonmonotonic, and almost the same when the surface is weakly hydrophilic or weakly hydrophobic (see Fig. 8). As already discussed, the selectivity of the surface is not important when a large amount of hydrophilic ions is present in its vicinity.

We have obtained the approximate analytical expression for the effective potential (see (37)-(40)), and it allows us to discuss the mutual effect of the charge distribution and the concentration profiles on the effective interactions. The two dominant terms decay as in Eq. (1), but with amplitudes depending on  $y$ . The amplitudes are the same as found previously for the correlation length larger than the screening length. The correction term decays as  $\propto \exp(-2\kappa L)$ .

We have found that when the surface with stronger selectivity is hydrophilic, the potential is more attractive, and when it is hydrophobic, the potential is more repulsive than predicted by (1). When the two identical confining surfaces are hydrophilic, then attraction between them can occur even when repulsion is expected from Eq. (1). When the two identical confining surfaces are hydrophobic, then repulsion between them can occur even when attraction is expected from Eq. (1).

The most spectacular violation of (1) is found when one surface is weakly hydrophobic and strongly charged, and the other surface is weakly charged and strongly selective. If the second surface is strongly hydrophilic and weakly charged, we obtain attraction, although both terms in (1) are repulsive. Such unexpected behavior was observed experimentally in Ref.[6]. If the second surface is weakly charged with opposite sign and it is strongly hydrophobic, we obtain repulsion, although both terms in (1) are attractive. Future experiments should verify this prediction.

Our findings can have numerous applications. For example, weakly hydrophobic, strongly charged substrate can be covered by a layer of oppositely charged, strongly hydrophobic particles away from  $\bar{T}_c$ . When  $\bar{T}_c$  is approached, the effective repulsion occurs and the particles are detached. On the other hand, strongly hydrophilic and similarly but weakly charged particles are repelled from the surface away from  $\bar{T}_c$ , but become attracted close to  $\bar{T}_c$ . We can thus control the coverage of the substrate. By changing temperature we can replace the hydrophobic layer of particles with opposite charge by the hydrophilic layer of particles with

the same charge as the bare substrate. Our results can have important consequences for mixtures of oppositely charged colloidal particles, which form ordered structures resembling ionic crystals in noncritical solvents [39]. In a mixture of strongly hydrophobic particles with small charge and weakly hydrophobic particles with large charge of opposite sign significant reversible restructuring is expected when  $\bar{T}_c$  is approached. The oppositely charged particles start to repel each other (Fig. 8), and the weakly charged strongly hydrophobic ones start to attract each other due to the Casimir potential. Different phase transitions can be induced by very small temperature changes. We are convinced that there can be many more applications of the control over the effective interactions. Our expressions can help to design the experimental studies.

## VII. ACKNOWLEDGMENTS

FP gratefully acknowledges A. Roostaei for his help in the numerical steps. The work of FP was realized within the International PhD Projects Programme of the Foundation for Polish Science, co-financed from European Regional Development Fund within Innovative Economy Operational Programme Grants for innovation. AC acknowledges partial financial support by the NCN grant 2012/05/B/ST3/03302.

## VIII. APPENDIX A EL EQUATIONS AND APPROXIMATE LANDAU-TYPE FUNCTIONAL

We consider the functional (3) in terms of the new variables (Eqs.(8),(10) and (11)), and with  $u_{vdW}$  given in Eq. (9). In the case of close packing

$$\sum_{i=1}^4 \frac{\mu_i \rho_i}{J} = \mu_0^* + \mu_\Phi^* \Phi + \mu_{ion}^* \rho_{ion} \quad (45)$$

where  $\mu_0^* = \frac{\mu_w + \mu_+}{2J}$ ,  $\mu_\Phi^* = \frac{\mu_w - \mu_l}{2J}$  and  $\mu_{ion}^* = \frac{\mu_+ - \mu_w}{J}$ . The entropy is given by

$$\begin{aligned} -\frac{Ts}{J} = \bar{T} \int_0^L dz & \left( \frac{1 - 2\rho_{ion}(z) + \Phi(z)}{2} \right) \ln \left( \frac{1 - 2\rho_{ion}(z) + \Phi(z)}{2} \right) \\ & + \left( \frac{1 - \Phi(z)}{2} \right) \ln \left( \frac{1 - \Phi(z)}{2} \right) + \left( \frac{\rho_{ion}(z) + \rho_q(z)}{2} \right) \ln \left( \frac{\rho_{ion}(z) + \rho_q(z)}{2} \right) \\ & + \left( \frac{\rho_{ion}(z) - \rho_q(z)}{2} \right) \ln \left( \frac{\rho_{ion}(z) - \rho_q(z)}{2} \right). \end{aligned} \quad (46)$$

In the bulk  $\rho_q = 0$ , and we restrict our attention to the critical composition  $\bar{\Phi} = 0$ . In thermodynamic equilibrium the number density of ions in the bulk,  $\bar{\rho}_{ion} = const.$ , satisfies the extremum condition for the grand potential, and from  $\frac{\partial \omega}{\partial \bar{\rho}_{ion}} = 0$  we obtain

$$\mu_{ion}^* = \bar{T} \ln R \quad (47)$$

where

$$R = \frac{\bar{\rho}_{ion}}{1 - 2\bar{\rho}_{ion}}. \quad (48)$$

On the other hand, in the presence of the external surface we obtain from the extremum condition  $\frac{\delta \omega}{\delta \rho_{ion}} = 0$

$$\mu_{ion}^* = \bar{T} \ln \left( \frac{\sqrt{\rho_{ion}^2(z) - \rho_q^2(z)}}{1 - 2\rho_{ion}(z) + \Phi(z)} \right). \quad (49)$$

By equating RHS of Eqs. (47) and (49) we obtain

$$\rho_{ion}(z) = \frac{-2R^2(1 + \Phi(z)) + \sqrt{\rho_q^2(z)(1 - 4R^2) + R^2(1 + \Phi(z))^2}}{1 - 4R^2}. \quad (50)$$

With the help of Eq. (50) we can eliminate  $\rho_{ion}(z)$  from (46). The remaining EL equations are obtained in a similar way, and have the forms

$$e\beta\psi(z) + \frac{1}{2} \ln \left( \frac{\rho_{ion}(z) + \rho_q(z)}{\rho_{ion}(z) - \rho_q(z)} \right) = 0, \quad (51)$$

and

$$\frac{d^2\Phi(z)}{dz^2} = -6\Phi + \frac{\bar{T}}{2} \ln \left[ \frac{1 - 2\rho_{ion}(z) + \Phi(z)}{(1 - \Phi(z))(1 - 2\rho_{ion}(z))} \right]. \quad (52)$$

Eqs.(50)-(52) and (6) form a closed set of two differential and two algebraic equations.

We introduce  $\vartheta = \rho_{ion}(z) - \bar{\rho}_{ion}$ , and assume that if the surface charge and the surface field are not large, then  $|\Phi| \ll 1$ ,  $|\rho_q| \ll 1$  and  $|\vartheta| \ll 1$ . Note that the internal energy is independent of  $\rho_{ion}$ . In order to calculate the excess grand potential associated with  $\vartheta$ , we need to calculate the excess of entropy and the excess of (45). Expanding (46), taking into account (47) and the analogous equation for  $\mu_{\Phi}^*$ , and keeping only the lowest-order terms we obtain

$$-\frac{T}{J}(s[\rho_q, \Phi, \rho_{ion}] - s[0, 0, \bar{\rho}_{ion}]) - (\mu_{\Phi}\Phi + \mu_{ion}\vartheta) \approx \bar{T} \int_0^L dz \left[ \frac{1}{1 - 2\bar{\rho}_{ion}} \left( \frac{1 - \bar{\rho}_{ion}}{2} \Phi^2(z) + \frac{1}{2\bar{\rho}_{ion}} \vartheta^2(z) - \Phi(z)\vartheta(z) \right) + \frac{\rho_q^2(z)}{2\bar{\rho}_{ion}^2} (\bar{\rho}_{ion} - \vartheta(z)) \right]. \quad (53)$$

Finally, by minimizing (53) with respect to the noncritical OP  $\vartheta(z)$  we obtain Eq. (14).

## IX. APPENDIX B. NONMONOTONIC $\Phi(z)$ IN SEMIINFINITE SYSTEM

From Eq. (28) we find that  $d\Phi(z)/dz = 0$  for real positive  $z$  when the surface field and the surface charge satisfy the condition

$$\frac{\bar{\rho}_{ion}h_0}{3\sigma_0^2} < \frac{y^2}{2y+1} < \frac{1}{3} \quad (54)$$

where  $\bar{T} \approx \bar{T}_c$  and  $y < 1$ .  $\Phi(z)$  assumes the extremum for

$$z = \frac{\xi}{2y-1} \ln \left( \frac{2yB\sigma_0^2}{H_0} \right). \quad (55)$$

When  $h_0 < 0$  the OP profile is nonmonotonic for  $y < 1/2$ , as discussed in sec.3a, and for  $y > 1/2$  if  $H_0 > 0$ , or explicitly

$$\frac{\bar{\rho}_{ion}h_0}{3\sigma_0^2} > -\frac{(1+2\kappa)y^2}{4y^2-1} \quad (56)$$

## X. APPENDIX C. THE CHARGE DISTRIBUTION

The coefficients in Eq. (32) are

$$\begin{cases} S_0 = \sigma_0 + \sigma_L e^{-\kappa L}, \\ S_L = \sigma_L + \sigma_0 e^{-\kappa L}, \\ S = 1 - e^{-2\kappa L}. \end{cases} \quad (57)$$

The explicit form of the charge-density profile with the effect of the critical adsorption included is (see Eqs.(25), (6) and (7))

$$\begin{aligned} \rho_q(z) = \frac{\kappa}{S} & \left[ a_0 e^{-\kappa z} + a_L e^{-\kappa(L-z)} - S_0 n_0 g_1 e^{-\kappa z} e^{-z/\xi} - S_L n_L g_1 e^{-\kappa(L-z)} e^{-(L-z)/\xi} \right. \\ & \left. + S_0 n_L g_2 e^{-\kappa z} e^{-(L-z)/\xi} + S_L n_0 g_2 e^{-\kappa(L-z)} e^{-z/\xi} \right], \end{aligned} \quad (58)$$

where

$$\begin{cases} a_0 = -S_0 + \frac{S_0 n_0}{S} g_3 + \frac{S_L}{S} [n_L g_3 - n_0 g_4] e^{-\kappa L} \left( 1 - e^{-L/\xi} \right) + \frac{S_0 n_L}{S} g_4 \left( e^{-L/\xi} - e^{-2\kappa L} \right), \\ a_L = -S_L + \frac{S_L n_L}{S} g_3 + \frac{S_0}{S} [n_0 g_3 - n_L g_4] e^{-\kappa L} \left( 1 - e^{-L/\xi} \right) + \frac{S_L n_0}{S} g_4 \left( e^{-L/\xi} - e^{-2\kappa L} \right), \end{cases} \quad (59)$$

$$\left\{ \begin{array}{l} g_1 = \frac{(1+y)^2}{(1+2y)}, \\ g_2 = \frac{(1-y)^2}{(2y-1)}, \\ g_3 = \frac{y(y+1)}{1+2y}, \\ g_4 = \frac{y(1-y)}{(2y-1)}, \end{array} \right. \quad (60)$$

$S_0$ ,  $S_L$  and  $S$  are given in (57), whereas  $n_0$  and  $n_L$  are given in Eqs.(61). (The correct expressions (32) and (58) differ from that given in Ref.[32] by terms  $O(e^{-2\kappa L})$ , which are negligible in the case of  $y \gg 1$  studied in Ref.[32].)

## XI. APPENDIX D. COEFFICIENTS IN EQ. (34)

The parameters in Eqs.(33) and (34) are

$$\left\{ \begin{array}{l} n_0 = \frac{1}{1+\xi^{-1}} \left[ h_0 - h_L \frac{1-\xi^{-1}}{1+\xi^{-1}} e^{-L/\xi} \right] \simeq_{\xi \rightarrow \infty} \left[ h_0 - h_L e^{-L/\xi} \right], \\ n_L = \frac{1}{1+\xi^{-1}} \left[ h_L - h_0 \frac{1-\xi^{-1}}{1+\xi^{-1}} e^{-L/\xi} \right] \simeq_{\xi \rightarrow \infty} \left[ h_L - h_0 e^{-L/\xi} \right]. \end{array} \right. \quad (61)$$

$$\begin{aligned} A_0(L) = & \frac{1}{1+\xi^{-1}} \left[ \left( 2(2\kappa+1)B - C \right) \sigma_0 \sigma_L e^{-\kappa L} - \frac{\xi-1}{\xi+1} \left( h_L + B\sigma_L^2(2\kappa+1) \right) e^{-L/\xi} \right. \\ & \left. + \left( (2\kappa+1)B(2\sigma_0^2 + \sigma_L^2) - (2\kappa-1)B\sigma_L^2 - C(\sigma_0^2 + \sigma_L^2) \right) e^{-2\kappa L} + \left( h_0 + (2\kappa+1)B\sigma_0^2 \right) \right], \end{aligned}$$

$$\begin{aligned} A_L(L) = & \frac{1}{1+\xi^{-1}} \left[ \left( 2(2\kappa+1)B - C \right) \sigma_0 \sigma_L e^{-\kappa L} - \frac{\xi-1}{\xi+1} \left( h_0 + B\sigma_0^2(2\kappa+1) \right) e^{-L/\xi} \right. \\ & \left. + \left( (2\kappa+1)B(2\sigma_L^2 + \sigma_0^2) - (2\kappa-1)B\sigma_0^2 - C(\sigma_0^2 + \sigma_L^2) \right) e^{-2\kappa L} + \left( h_L + (2\kappa+1)B\sigma_L^2 \right) \right], \end{aligned} \quad (62)$$

where  $B$  is defined in Eq. (30),

$$Q(L) = \frac{B}{(1 - e^{-2\kappa L})^2} \simeq B(1 + 2e^{-2\kappa L}), \quad (63)$$

and

$$C = \frac{\bar{T}y^2}{\bar{\rho}_{ion}} \approx \frac{6y^2}{\bar{\rho}_{ion}}. \quad (64)$$

The RHS in the above equation is valid for  $\bar{T} \approx \bar{T}_c$ , and we have used the MF result  $\bar{T}_c = 6$ .

## XII. APPENDIX E. COEFFICIENTS IN EQ. (41)

$$A_\kappa = \sigma_0 \sigma_L \left[ 2 - \frac{3}{4}(h_0 + h_L) \right] \quad (65)$$

$$B_{2\kappa} = \sigma_0^2 + \sigma_L^2 - \frac{4\bar{\rho}_{ion}h_0h_L}{\bar{T}} - \frac{3(\sigma_0^2h_0 + \sigma_L^2h_L)}{4} - \frac{(\sigma_0^2h_L + \sigma_L^2h_0)}{2}\kappa L \quad (66)$$

- 
- [1] C. N. Likos, *Phys. Rep.* **348**, 267 (2001).
  - [2] L. Belloni, *J. Phys.:Cond. Mat* **12**, R549 (2000).
  - [3] C. Hertlein, L. Helden, A. Gambassi, S. Dietrich, and C. Bechinger, *Nature* **451**, 172 (2008).
  - [4] A. Gambassi, A. Maciolek, C. Hertlein, U. Nellen, L. Helden, C. Bechinger, and S. Dietrich, *Phys. Rev. E* **80**, 061143 (2009).
  - [5] D. Bonn, J. Otwinowski, S. Sacanna, H. Guo, G. Wegdam, and P. Schall, *Phys. Rev. Lett* **103**, 156101 (2009).
  - [6] U. Nellen, J. Dietrich, L. Helden, S. Chodankar, K. Nygard, J. F. van der Veen, and C. Bechinger, *Soft Matter* **80**, 061143 (2011).
  - [7] V. D. Nguyen, S. Faber, Z. Hu, G. H. Wegdam, and P. Schall, *Nature Communications* **4**, 1584 (2013).
  - [8] S. L. Veatch, O. Soubias, S. L. Keller, and K. Gawrisch, *Proc. Nat. Acad. Sci. USA* **104**, 17650 (2007).
  - [9] B. B. Machta, S. L. Veatch, and J. P. Sethna, *Phys. Rev. Lett* **109**, 138101 (2012).
  - [10] A. R. Honerkamp-Smith, S. L. Veatch, and S. L. Keller, *Biochimica et Biophysica Acta* **1788**, 53 (2009).
  - [11] H. W. Diehl, *Field-theoretic Approach to Critical Behavior at Surfaces*, vol. 10 of *Phase Transitions and Critical Phenomena* (Academic Press, London, 1986), 1st ed., pages 75-267.



- [12] M. E. Fisher and P. G. de Gennes, *C. R. Acad. Sci. Ser. B* **287**, 207 (1978).
- [13] M. Krech, *Casimir Effect In Critical Systems* (World Scientific, Singapore, 1994).
- [14] M. Krech, *J. Phys.:Cond. Mat* **11**, R391 (1999).
- [15] R. Piazza, S. Buzzaccaro, A. Parola, and J. Colombo, *J. Phys.:Cond. Mat* **23**, 194114 (2011).
- [16] B. S. Pradip, V. D. Nguyen, A. V. Limaye, and P. Schall, *Advanced Materials* **25**, 14991503 (2013).
- [17] J. L. Barrat and J.-P. Hansen, *Basic Concepts for Simple and Complex Liquids* (Cambridge University Press, 2003).
- [18] O. Vasilyev, A. Maciołek, , and S. Dietrich, *Phys. Rev. E* **84**, 041605 (2010).
- [19] A. Maciołek, A. Ciach, and A. Drzewiński, *Phys. Rev. E* **60**, 2887 (1999).
- [20] A. Ciach and U. Ritschel, *Nucl. Phys. B* **489**, 653 (1997).
- [21] D. B. Abraham and A. Maciołek, *Phys. Rev. E* **105**, 055701 (2010).
- [22] J. N. Israelachvili, *Intermolecular and Surface Forces* (Academic Press, London, 1985).
- [23] B. Derjaguin, *Kolloid Zeitschrift* **69**, 155 (1934).
- [24] A. Stradner, H. Sedgwick, F. Cardinaux, W. Poon, S. Egelhaaf, and P. Schurtenberger, *Nature* **432**, 492 (2004).
- [25] A. Imperio and L. Reatto, *J. Chem. Phys* **124**, 164712 (2006).
- [26] A. J. Archer, *Phys. Rev. E* **78**, 031402 (2008).
- [27] A. de Candia, E. DelGado, A. Fierro, N. Sator, M. Tarzia, and A. Coniglio, *Phys. Rev. E* **74**, 010403(R) (2006).
- [28] A. Ciach, *Phys. Rev. E* **78**, 061505 (2008).
- [29] A. Ciach and W. T. Gózdź, *Condensed Matter Physics* **13**, 23603 (2010).
- [30] A. Ciach and A. Maciolek, *Phys. Rev. E* **81**, 041127 (2010).
- [31] F. Pousaneh and A. Ciach, *J. Phys.:Cond. Mat* **23**, 412001 (2011).
- [32] F. Pousaneh, A. Ciach, and A. Maciołek, *Soft Matter* **8**, 7567 (2012).
- [33] M. Bier, A. Gambassi, M. Oettel, and S. Dietrich, *Europhys Lett* **95**, 60001 (2011).
- [34] M. Bier, A. Gambassi, and S. Dietrich, *J. Chem. Phys* **137**, 034504 (2013).
- [35] S. Samin and Y. Tsori, *Europhys Lett* **95**, 36002 (2011).
- [36] S. Samin and Y. Tsori, *J. Chem. Phys* **136**, 154908 (2012).
- [37] J. N. Israelachvili, *Intermolecular and Surface Forces (Third Edition)* (Academic Press, Boston, 2011).

- [38] T. F. Mohry, A. Maciolek, , and S. Dietrich, *Phys. Rev. E* **81**, 061117 (2010).
- [39] M. Leunissen, C. Christova, A.-P. Hynninen, C. Royal, A. Campbell, A. Imhof, M. Dijkstra, R. van Roji, and A. van Blaaderen, *Nature* **437**, 235 (2005).